

# CMS-LSTM: CONTEXT EMBEDDING AND MULTI-SCALE SPATIOTEMPORAL EXPRESSION LSTM FOR PREDICTIVE LEARNING

Zenghao Chai<sup>1</sup>, Zhengzhuo Xu<sup>1</sup>, Yunpeng Bai<sup>1</sup>, Zhihui Lin<sup>1</sup>, Chun Yuan<sup>1,2</sup>

<sup>1</sup>Shenzhen International Graduate School, Tsinghua University, <sup>2</sup>Peng Cheng Laboratory  
zenghaochai@gmail.com, {xzz20, byp20, lin-zh14}@tsinghua.edu.cn, yuanc@sz.tsinghua.edu.cn

## ABSTRACT

Spatiotemporal predictive learning (ST-PL) is a hotspot with numerous applications, such as object movement and meteorological prediction. It aims at predicting the subsequent frames via observed sequences. However, inherent uncertainty among consecutive frames exacerbates the difficulty in long-term prediction. To tackle the increasing ambiguity during forecasting, we design CMS-LSTM to focus on context correlations and multi-scale spatiotemporal flow with details on fine-grained locals, containing two elaborate designed blocks: Context Embedding (CE) and Spatiotemporal Expression (SE) blocks. CE is designed for abundant context interactions, while SE focuses on multi-scale spatiotemporal expression in hidden states. The newly introduced blocks also facilitate other spatiotemporal models (e.g., PredRNN, SA-ConvLSTM) to produce representative implicit features for ST-PL and improve prediction quality. Qualitative and quantitative experiments demonstrate the effectiveness and flexibility of our proposed method. With fewer params, CMS-LSTM outperforms state-of-the-art methods in numbers of metrics on two representative benchmarks and scenarios. Code is available at <https://github.com/czh-98/CMS-LSTM>.

**Index Terms**— Spatiotemporal predictive learning, context embedding, multi-scale attention, fine-grained details

## 1. INTRODUCTION

Spatio-Temporal Predictive Learning (ST-PL) is one of the hotspots in predictive learning with broad research prospects in computer vision. The core task and challenge are predicting future sequences based on limited observed frames, containing a large amount of visual information and profound dynamic changes. Recent years have seen significant progress in ST-PL. Numerous researchers have carried out in-depth research and proposed a series of RNNs [1] (especially LSTMs) based models, from the original ConvLSTM [2, 3] used for precipitation nowcasting to the improved approaches, such as PredRNN [4, 5], PredRNN++ [6], MIM [7], E3D-LSTM [8], SA-ConvLSTM [9]. These methods have achieved remarkable results in ST-PL.

LSTM based models are mainstream in ST-PL. However, the input and context of previous models are solely correlated by CNN layers and channel-wise addition operation. Hence, with the increase of models' depth, correlations between the current input and upper context will decline as information flows through layers. To improve the correlation and capture important parts of input and context, we design Context Embedding (CE) block to re-weight input and context states in an iteratively interacted mode to reflect the spatiotemporal details. CE block utilizes lightweight CNN layers to iteratively focus on important parts for subsequent prediction to enhance the correlations and capture the variation trend.

Spatiotemporal sequences contain complex semantic features, whereas the certainty of frames is exceptionally fuzzy. Previous work predicts increasingly blur details because they do not balance focusing on the changed regions and weakening the expression on unchanged parts. Instead, they merely concentrate on global spatiotemporal flows of given frames in hidden states, resulting in more extra params and ignorance of fine-grained variations. We creatively divide latent states into multi-scales to capture details of specific regions in parallel by proposing Multi-Scale Spatiotemporal Expression (SE) block. SE block captures fine-grained details based on the self-attention mechanism, which improves the dominant changed regions well expressed and simultaneously weakens the negligible parts with lower expression.

We integrate CE and SE blocks by proposing Context Embedding and Multi-Scale Spatiotemporal Expression LSTM (CMS-LSTM), an extension structure of ConvLSTM to improve prediction quality especially the details. CMS-LSTM overcomes deficiencies of the isolated relationship of context and input and pays more attention to multi-scale spatiotemporal flows. The main contributions are as follows:

- We design CE block and SE block to capture fine-grained details to promote prediction quality. CE block maintains consistency and extracts further correlations between the current input and upper context. SE block facilitates multi-scale dominant spatiotemporal flows' expression and weakens the negligible parts simultaneously.
- To the best of our knowledge, the proposed CMS-LSTM is the first to innovatively integrate context interaction enhancement and multi-scale spatiotemporal expression

mechanism for detailed prediction. It achieves significant improvement and state-of-the-art results in numbers of metrics on two representative benchmarks and scenarios.

- Qualitative and quantitative experiments have demonstrated the importance of context interactions and multi-scale spatiotemporal flows in ST-PL. The proposed CE block and SE block have the portability to transplant in other models.

## 2. METHODS

### 2.1. Overview of CMS-LSTM

Considering the limitation of ConvLSTM, the core goals of CMS-LSTM are to maintain the spatiotemporal consistency and correlations among frames in LSTM layers, facilitate multi-scale dominant spatiotemporal flows' expression and weaken the negligible ones simultaneously. In specific, CMS-LSTM is constructed by taking both considerations of context interactions and multi-scale spatiotemporal flows.

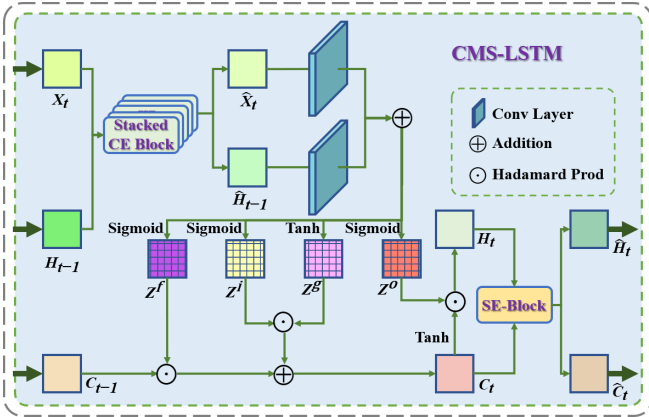


**Fig. 1:** Architecture of CMS-LSTM.  $H_{t-1}$  and  $C_{t-1}$  represent output state and memory state of  $t-1$  time respectively,  $X_t$  represents the  $t$  time input.  $\hat{H}_t$  and  $\hat{C}_t$  are the output of CMS-LSTM, i.e., the output state and memory state of  $t$  time.

The architecture of proposed CMS-LSTM is illustrated in Fig. 1. Formally, the calculation process of CMS-LSTM can be expressed as follows:

$$\begin{aligned}
\hat{X}_t, \hat{H}_{t-1} &= CE(\dots CE(X_t, H_{t-1})) \\
g_t &= \tanh(W_{xg} \star \hat{X}_t + W_{hg} \star \hat{H}_{t-1} + b_g) \\
i_t &= \sigma(W_{xi} \star \hat{X}_t + W_{hi} \star \hat{H}_{t-1} + b_i) \\
f_t &= \sigma(W_{xf} \star \hat{X}_t + W_{hf} \star \hat{H}_{t-1} + b_f) \\
C_t &= f_t \circ C_{t-1} + i_t \circ g_t \\
o_t &= \sigma(W_{xo} \star \hat{X}_t + W_{ho} \star \hat{H}_{t-1} + b_o) \\
H_t &= o_t \circ \tanh(C_t) \\
\hat{H}_t, \hat{C}_t &= SE(H_t, C_t)
\end{aligned} \tag{1}$$

In Eq. 1.  $\hat{X}_t$  and  $\hat{H}_{t-1}$  represent the output of  $n$  stacked CE blocks with intensive context interactions. Then,  $H_t$  and  $C_t$

are obtained through LSTM gate operations, which merely contain limited global spatiotemporal flows at present. We thus adopt 3-scale SE block to extract multi-scale features for further spatiotemporal flows among neighbors, to obtain the final output  $\hat{H}_t$  and  $\hat{C}_t$  of CMS-LSTM. The structure of CE and SE blocks will be introduced later.

### 2.2. CE Block

Rethinking the process of ConvLSTM [2], the input state  $X_t$  and previous output state  $H_{t-1}$  only interact separately by a CNN layer and addition operation. Limited interaction between the two states is crucial for the model's information loss and blurry prediction results. When the two states are completely independently entering into subsequent LSTM parts, correlations between the current input and upper context is bound to disappear as models become increasingly complex.

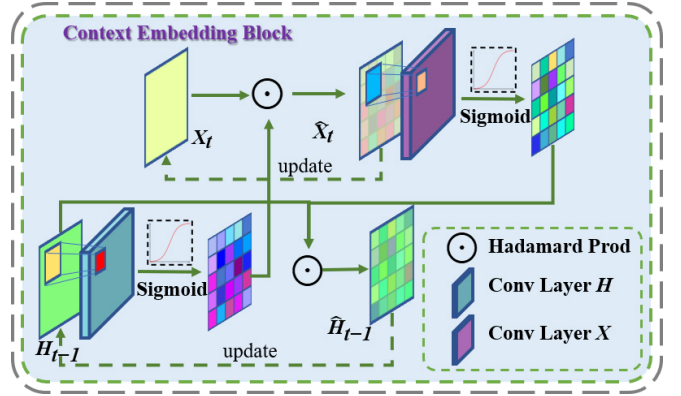


**Fig. 2:** The pipeline of proposed CE block, where  $H_{t-1}$ ,  $X_t$  are the previous state and current input, respectively.  $H$  and  $X$  are  $5 \times 5$  convolution layers to extract features of  $H_t$  and  $\hat{X}_t$ , respectively.  $\hat{H}_{t-1}$  and  $\hat{X}_t$  are the output of CE block, representing the previous state and current input after context embedding, respectively.

On the top of aforementioned, the current ConvLSTM and its extensions are incapable of re-weighting or capturing the important parts for the next timestamp. Therefore, we design CE block that contains additional operations to make persistent correlations of  $X_t$  and  $H_{t-1}$ , to minimize the correlation decrease passing through LSTM layers and achieve a lasting relationship for better predicting performance. To achieve this, we utilize spatiotemporal features to generate a context weight map to enforce important information well captured, i.e., to concentrate on the changed parts while simultaneously weakening the fixed parts. Specifically, CE block (see Fig. 2) consists of the following steps:

**Step1.** To capture the important parts of current input that are helpful for long-term prediction, we generate a weight map of upper context via a  $5 \times 5$  kernel CNN layer to capture the context features, which indicates the potential movement trend in the following time stamp. Then, we adopt *Sigmoid* function to normalize the weight map into  $(0, 1)$ , and

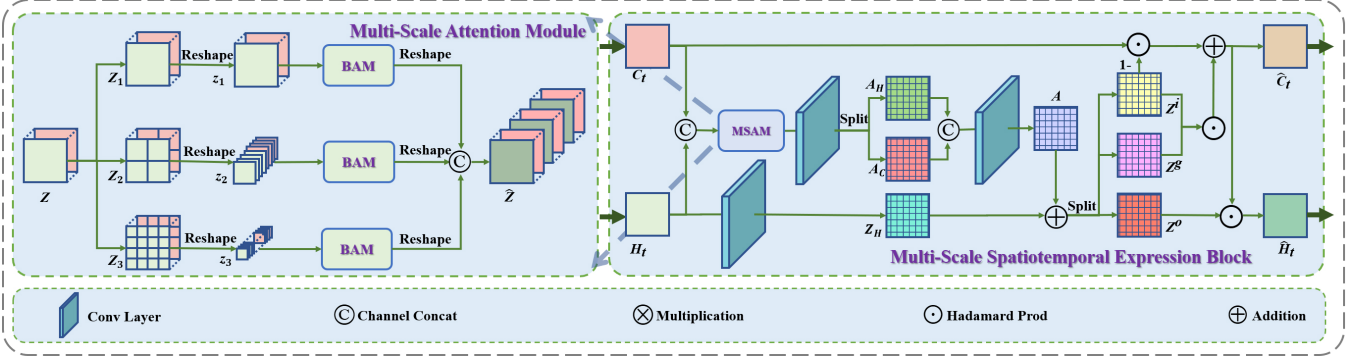


**Fig. 3:** The pipeline of proposed SE block, with sub-module in the left part named **Multi-Scale Attention Module (MSAM)**, where  $H_t$  and  $C_t$  represent the output of original ConvLSTM, and  $5 \times 5$  convolution layers are used to extract features,  $\hat{H}_t$  and  $\hat{C}_t$  represent the output state and memory state after multi-scale spatiotemporal flows' extraction.

re-weight the input feature  $X_t$  by the Hadamard product to highlight the important part of the input state. Finally, we multiply the weight map by a constant scale factor  $s$  to avoid getting increasingly smaller as CE blocks stacked.

**Step2.** To enforce the context feature well absorb in the changing trend of current input frames, i.e., consider the current motion and weaken the unchanged parts with lower expression. We update  $H_{t-1}$  by multiplying an input-related weight map to extract the subsequent motion concentration for subsequent prediction by the Hadamard product. The weight map has the same generation mode in Step 1, i.e., capture the local context motion features by a CNN layer and activation function with scale factor. Then, the updated context state  $\hat{H}_{t-1}$  and input state  $\hat{X}_t$  is obtained.

Formally, context correlations are extracted by the interaction mode as Eq. 2 in the proposed CE block, where  $W_H, W_X$  are CNN and  $\sigma$  represents *Sigmoid* operation.

$$\begin{aligned} \hat{X}_t &= s \times \sigma(W_H \star H_{t-1} + b_H) \circ X_t \\ \hat{H}_{t-1} &= s \times \sigma(W_X \star \hat{X}_t + b_X) \circ H_{t-1} \end{aligned} \quad (2)$$

To achieve richer interactions and minimize the extra params, we use stacked weight-shared CE blocks to extract abundant correlation further.

### 2.3. SE Block

We find it's common that the prediction results of models become increasingly blur especially in the edges and details. The reason is that previous LSTM-based approaches mainly concentrate on modeling global spatiotemporal features and flows, regardless of multi-scale neighbor features among sequences. We emphasize the insufficiency of previous work in multi-scale spatiotemporal flow extractions and construct SE block for maximizing extract multi-scale implicit spatiotemporal flows to overcome previous weakness.

Considering those aforementioned, we construct SE block to enable the output state  $H_t$  and memory state  $C_t$  to contain abundant fine-grained spatiotemporal information. The

pipeline of SE block is illustrated in Fig. 3, which can be summarized as the following two steps.

**Step1. Multi-Scale Spatiotemporal Features Expression** To extract fine-grained spatiotemporal features in latent states, we adopt self-attention mechanism to obtain local features of specific scales. To avoid additional computation load and params on two hidden states, we stack the spatiotemporal states  $H_t, C_t \in \mathbb{R}^{C \times H \times W}$  into  $Z \in \mathbb{R}^{C \times H \times W \times 2}$  to improve the parallel efficiency.

To capture fine-grained feature in specific scale, we divide  $Z$  into  $n$  multi-scale groups  $\{Z_1, \dots, Z_n\}$  according to segmentation rules  $R = \{R_1, \dots, R_n\}$ , then each  $Z_i, i \in [1, n]$  is stacked in  $C$  channel to compose  $\{z_1, \dots, z_n\}$ . For each  $z_i, i \in [1, n]$ , we use standard self-attention module to reflect the importance of representing spatiotemporal characteristics of different regions, and denote as:

$$\begin{aligned} Z_i &= \underset{R_i \in R}{\text{DIVIDE}}([H_t, C_t]) \quad i \in [1, n] \\ \hat{z}_i &= \underset{C}{\text{BAM}}(\underset{C}{\text{STACK}}(Z_i)) \quad i \in [1, n] \end{aligned} \quad (3)$$

Where BAM is a standard self-attention operation, which uses  $1 \times 1$  CNN layers to map  $z_i$  into  $K, Q, V$  and obtains updated  $\hat{z}_i$  as follows:

$$\text{BAM}(z_i) \triangleq \text{Softmax}(Q^T \times K) \times V + z_i \quad (4)$$

After that, the multi-scale latent features are restored in  $H$  and  $W$  channels to recover the original shape, then we concat these multi-scale features in  $C$  channel to composing  $\hat{Z} \in \mathbb{R}^{n \times C \times H \times 2 \times W}$ . Ultimately, feature maps  $A_H, A_C \in \mathbb{R}^{n \times C \times H \times W}$  are calculated by  $5 \times 5$  CNN layer taking  $\hat{Z} \in \mathbb{R}^{n \times C \times H \times W \times 2}$  as input and separated in the last channel.

$$\begin{aligned} \hat{Z} &= \underset{C}{\text{CONCAT}}(\underset{R_i \in R}{\text{RESTORE}}(\hat{z}_i)) \quad i \in [1, n] \\ [A_H, A_C] &= \text{SEPARATE}(W_Z \star \hat{Z} + b_z) \end{aligned} \quad (5)$$

We successfully obtain the fine-grained features  $A_H$  and  $A_C$ . They consist of abundant spatiotemporal correlations and details of the previous two states.

**Step2. Spatiotemporal Implicit States Update** We utilize  $A_H, A_C$  to update latent states with abundant details. Specifically, we stack the spatiotemporal related latent feature into channel dim and follow by a  $5 \times 5$  CNN layers, then split into 3 parts:  $Z^i, Z^g$ , and  $Z^o$ , respectively.

$$\begin{aligned} i_t &= \sigma(W_{Ai} \star [A_H, A_C] + W_{hi} \star Z_H + b_i) \\ g_t &= \tanh(W_{Ag} \star [A_H, A_C] + W_{hg} \star Z_H + b_g) \\ o_t &= \sigma(W_{Ao} \star [A_H, A_C] + W_{ho} \star Z_H + b_o) \end{aligned} \quad (6)$$

Then, the memory state  $\hat{C}_t$  and output state  $\hat{H}_t$  integrate the detailed multi-scale features and further updated as follows:

$$\begin{aligned} \hat{C}_t &= (1 - i_t) \circ C_t + i_t \circ g_t \\ \hat{H}_t &= o_t \circ \hat{C}_t \end{aligned} \quad (7)$$

With the construction of SE block, memory state and output state focus more on the detailed sequence changes in the long-term prediction and can effectively counter the gradually fuzzy prediction results.

### 3. EXPERIMENTS

#### 3.1. Implementation Details

We use the same 4-layer LSTM architecture with 64 hidden states for fair comparisons. Setting mini-batch to 8 and initial learning rate to 0.001, scheduled sampling [10] and layer normalization [11] are simultaneously adopted during training. We use  $L_1 + L_2$  loss with AdamW [12] optimizer to train the model, We set scale factor of CE as  $s = 2$ .

#### 3.2. Datasets

**Moving MNIST** Moving MNIST [13] is a common benchmark in ST-PL, depicting 2 digits' movement with constant velocity. Each data contains  $64 \times 64 \times 1$  consecutive frames with 10 for input and 10 for prediction, 10,000 randomly generate sequences for training and 10,000 fixed sequences for testing.

**Typhoon** Typhoon dataset is distributed by CEReS [14]. We normalize the radar observation data into  $[0, 1]$ , resize the image to  $64 \times 64 \times 1$ . Each frame represents meteorological observation in the past 1 hour. We use the given 8-hour observation data to predict the next 4 hours, with 1809 sequences for training and 603 sequences for testing.

#### 3.3. Comparisons with SOTA Methods

We compare the proposed model with previous SOTA methods quantitatively and qualitatively to demonstrate our method's advantages and effectiveness.

**Results on Moving MNIST** We set 80,000 iterations consistent with [4, 9] and 400,000 iterations for better performance. Quantitative and qualitative comparisons are shown

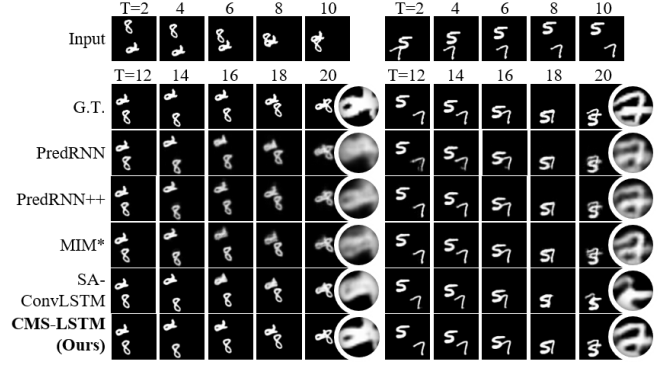


**Fig. 4:** Qualitative comparisons of previous models on Moving MNIST test set at 80,000 iterations. The output frames are shown at one-frame intervals. We magnify the local of prediction results for detailed comparisons at the last frame.

**Table 1:** Quantitative comparisons of previous SOTA models on Moving MNIST test set. All models predict 10 frames by observing 10 previous frames. We also train 400,000 iterations (CMS-LSTM\*) for higher performance.

Models	#Params	PSNR $\uparrow$	SSIM $\uparrow$	MSE $\downarrow$	MAE $\downarrow$
DDPAE [15]	-	21.170	0.922	38.9	90.7
CrevNet [16]	-	-	0.928	38.5	-
PhyDNet [17]	-	23.120	0.947	24.4	70.3
PDE-Driven [18]	-	21.760	0.909	-	-
PredRNN [4]	13.799 M	19.603	0.867	56.8	126.1
PredRNN++ [6]	13.237 M	20.239	0.898	46.5	106.8
MIM* [7]	27.971 M	20.678	0.910	44.2	101.1
E3D-LSTM [8]	38.696 M	20.590	0.910	41.7	87.2
SA-ConvLSTM [9]	10.471 M	20.500	0.913	43.9	94.7
CMS-LSTM	7.968 M	21.955	0.931	33.6	73.1
<b>CMS-LSTM*</b>	<b>7.968 M</b>	<b>23.682</b>	<b>0.949</b>	<b>24.3</b>	<b>58.1</b>

in Tab. 1 and Fig. 4, respectively. PSNR, SSIM, MSE, and MAE are used for quantitative comparisons. The performance improves as the SSIM and PSNR increase and the MSE and MAE decrease. Results in Tab. 1 demonstrate the superiority of our method on Moving MNIST dataset in all above metrics, improving 14.5% and 3.9% on PSNR and SSIM, and reducing 41.7% and 33.4% on MSE and MAE respectively compared with SA-ConvLSTM [9].

Results in Fig. 4 show that CMS-LSTM has better capability to capture variations over digits, especially deals with the trajectory of overlap digits and maintains the clarity over time. In contrast, predicted frames of other methods appear blurry in the digits and fail to deal with overlap digits.

**Results on Typhoon** We train the proposed models for 100,000 iterations and make fair comparisons with previous methods. PSNR, SSIM, MSE, and MAE are adopted to evaluate these models' performance qualitatively and quantitatively, corresponding to Fig. 5 and Tab. 2.

The proposed method outperforms existing techniques quantitatively in Tab. 2 and qualitatively in Fig. 5. CMS-LSTM is the only model that performs well in the detail texture of frames, i.e., it can preserve and predict the potential trend of meteorological information.

Results in Tab. 2 demonstrate the superiority of the pro-



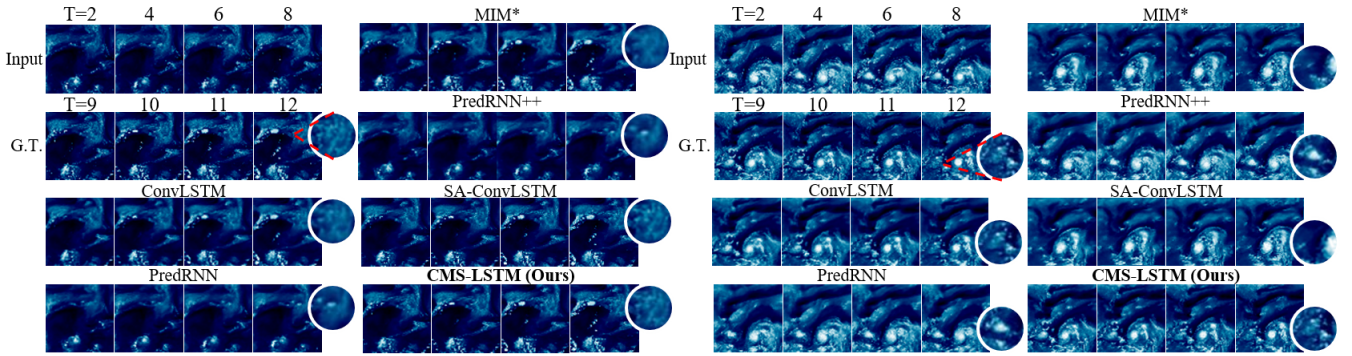


**Fig. 5:** Qualitative comparisons of previous SOTA models on Typhoon test set. The output frames are shown at one-frame intervals. We frame the local of predicted results for additional detailed comparisons at the last frame.

**Table 2:** Quantitative comparisons of previous SOTA models on Typhoon test set. All models predict the next 4 frames (atmosphere trends for the next 4 hours) via 8 observed meteorological data. We also use  $7 \times 7$  convolution layers (denoted as CMS-LSTM#) for higher performance.

Models	PSNR $\uparrow$	SSIM $\uparrow$	MSE $\downarrow$	MAE $\downarrow$
ConvLSTM [2]	26.353	0.851	10.43	119.6
PredRNN [4]	27.637	0.887	7.71	107.3
PredRNN++ [6]	28.287	0.891	6.72	114.5
MIM* [7]	26.721	0.893	9.14	132.2
SA-ConvLSTM [9]	28.456	0.898	7.07	94.2
CMS-LSTM	28.891	0.907	6.24	86.4
<b>CMS-LSTM#</b>	<b>30.207</b>	<b>0.921</b>	<b>5.21</b>	<b>76.0</b>

posed method, with better spatiotemporal expression and prediction results, which further proves the tremendous necessity of interactions among latent states in ST-PL.

## 4. ABLATION STUDIES

### 4.1. Weight Map Visualization

To illustrate the effectiveness of the proposed methods, we visualized the weight map calculated by CE and SE block in the last LSTM layer and randomly choose some examples from the test set of Moving MNIST as illustrated in Fig. 6.

The weight map shows the important part of among frames. CE block enables important parts closely related to the context (e.g., moving trends) and input frames to be well captured, revealing the rough candidate regions as shown warmer color and keeping the unchanged parts with a lower weight. The output frames are closely related to the weight map where the important part is captured by SE block. SE block captures fine-grained details for prediction, which can alleviate the fuzzy texture in long-term prediction, especially in the challenge overlap cases. CMS-LSTM still accurately capture important parts and make satisfactory results.

As shown in Fig. 6, CE block is effective in capturing a potential changed part, the larger weight that urges models to focus on these regions and ignore the fixed unchanged part, to avoid the wrong prediction results. The context embedding mode effectively predicts the potential trend of current

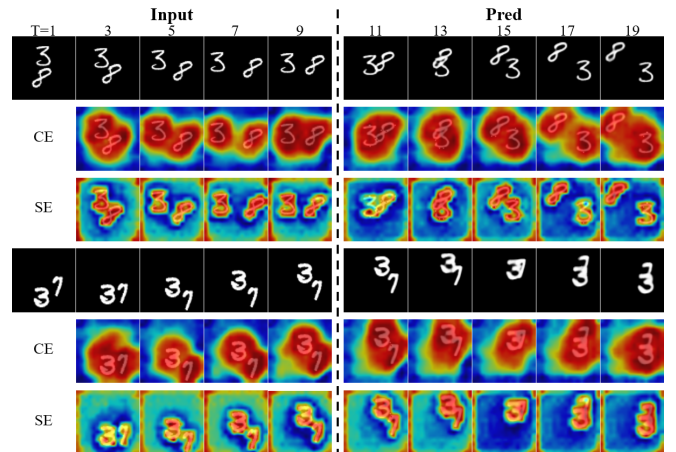


**Fig. 6:** Visualization of the proposed blocks on Moving MNIST test set of the last LSTM layer, where the warm colors indicate higher weights. The proposed methods enable capturing important regions for better prediction.

input and upper context and effectively weakens the expression of irrelevant parts in the process of sequences. In SE block, the updated latent states are more focused on important parts, which helps the prediction results of the model to achieve higher prediction quality.

### 4.2. Ablation Study of CMS-LSTM

We conduct ablation studies to verify the effectiveness of CE and SE block. Experiments below set 80,000 (100,000) iterations in Moving MNIST (Typhoon) for training.

We verify the necessity of context interactions and multi-scale spatiotemporal flows by comparing CMS-LSTM removing CE and SE, respectively, and then using different scales to illustrate the necessity of the multi-scale spatiotemporal expression. The entire CMS-LSTM achieves the best performance compared with the original ConvLSTM. Comparing models with and without CE block demonstrates the necessity of context interactions. Moreover, experiments in multi-scale further show the importance of spatiotemporal flow extractions in different scales.

Besides, to testify the portability of CE and SE, we transplant them into previous SOTA methods. Specifically, we

**Table 3:** Ablation studies on Moving MNIST and Typhoon datasets. Models with and without CE block or SE block are tested sequentially in different backbones, as well as SE block with different scales in ConvLSTM.

Models	Moving MNIST								Typhoon							
	PSNR $\uparrow$	$\Delta$	SSIM $\uparrow$	$\Delta$	MSE $\downarrow$	$\Delta$	MAE $\downarrow$	$\Delta$	PSNR $\uparrow$	$\Delta$	SSIM $\uparrow$	$\Delta$	MSE $\downarrow$	$\Delta$	MAE $\downarrow$	$\Delta$
ConvLSTM	18.523	-	0.877	-	70.4	-	115.9	-	26.353	-	0.851	-	10.4	-	119.6	-
w CE, w/o SE	21.189	+2.666	0.918	+0.041	39.1	-31.3	82.8	-33.1	<b>29.022</b>	<b>+2.669</b>	0.906	+0.055	6.32	-4.08	87.0	-32.6
w CE, w 1-scale SE	21.708	+3.185	0.927	+0.050	35.1	-35.3	76.3	-39.6	28.785	+2.432	0.903	+0.052	6.58	-3.82	89.3	-30.3
w CE, w 2-scale SE	21.858	+3.335	0.929	+0.052	33.8	-36.6	74.3	-41.6	28.650	+2.297	0.901	+0.050	6.75	-3.65	90.5	-29.1
w/o CE, w SE	21.712	+3.189	0.927	+0.050	34.8	-35.6	76.2	-39.7	28.555	+2.202	0.899	+0.048	6.86	-3.54	92.1	-27.5
w CE, w SE	<b>21.955</b>	<b>+3.432</b>	<b>0.931</b>	<b>+0.054</b>	<b>33.6</b>	<b>-36.8</b>	<b>73.1</b>	<b>-42.8</b>	28.891	+2.538	<b>0.907</b>	<b>+0.056</b>	<b>6.24</b>	<b>-4.16</b>	<b>86.4</b>	<b>-33.2</b>
PredRNN	19.603	-	0.867	-	56.8	-	126.1	-	27.637	-	0.887	-	7.71	-	107.3	-
w CE, w/o SE	22.356	+2.753	0.924	+0.057	30.7	-26.1	82.7	-43.4	28.061	+0.424	0.896	+0.009	7.06	-0.65	102.7	-4.60
w/o CE, w SE	22.761	+3.158	0.931	+0.064	28.7	-28.1	76.9	-49.2	28.516	+0.879	0.900	+0.013	6.51	-1.20	<b>90.3</b>	<b>-17.0</b>
w CE, w SE	<b>23.210</b>	<b>+3.607</b>	<b>0.935</b>	<b>+0.068</b>	<b>26.3</b>	<b>-30.5</b>	<b>74.2</b>	<b>-51.9</b>	<b>28.864</b>	<b>+1.227</b>	<b>0.907</b>	<b>+0.020</b>	<b>6.03</b>	<b>-1.68</b>	94.7	-12.6
SA-ConvLSTM	20.500	-	0.913	-	43.9	-	94.7	-	28.456	-	0.898	-	7.07	-	94.2	-
w CE, w/o SE	<b>22.591</b>	<b>+2.091</b>	<b>0.929</b>	<b>+0.016</b>	<b>27.3</b>	<b>-16.6</b>	79.0	-15.7	28.628	+0.172	0.900	+0.002	6.88	-0.19	89.3	-4.90
w/o CE, w SE	21.700	+1.200	0.928	+0.015	34.8	-9.10	<b>75.7</b>	<b>-19.0</b>	28.690	+0.234	0.903	+0.005	6.62	-0.45	89.4	-4.80
w CE, w SE	21.659	+1.159	0.927	+0.014	34.7	-9.20	76.4	-18.3	<b>29.505</b>	<b>+1.049</b>	<b>0.913</b>	<b>+0.015</b>	<b>5.82</b>	<b>-1.25</b>	<b>82.5</b>	<b>-11.7</b>

compare PredRNN [4] and SA-ConvLSTM [9] with/without CE block and SE block in the same experiment settings for quantitative comparisons on Moving MNIST and Typhoon dataset, results shown in Tab. 3. Tab. 3 further verifies the portability of the proposed blocks. With the transplant of them, previous models’ performances do get significantly improved, indicating the ability of our methods to be transplanted in other spatiotemporal predictive models.

## 5. CONCLUSIONS

This paper creatively proposes effective modules named CE block and SE block focused on context interactions and multi-scale spatiotemporal expression, and then constructs CMS-LSTM. Qualitative and quantitative experiments demonstrate the superiority of our method dealing with uncertainty and overlap in sequences, showing state-of-the-art performance on representative datasets.

Ablation studies further verify the effectiveness and flexibility of our method. CE block can maintain the spatiotemporal consistency among long sequences, and SE block facilitates multi-scale dominant spatiotemporal flows’ expression and simultaneously weakens the negligible ones. Moreover, they can transplant to other spatiotemporal predictive related models to improve the performance markedly.

## 6. ACKNOWLEDGMENT

This work is supported by NSFC project Grant No. U1833101, SZSTI Grant No. JCYJ20190809172201639, WDZC20200820200655001. Tsinghua & Tencent Joint Research Laboratory.

## 7. REFERENCES

- [1] S. Hochreiter and J. Schmidhuber, “Long short-term memory,” *Neural computation*, 1997.
- [2] X. Shi, Z. Chen, H. Wang, et al., “Convolutional lstm network: A machine learning approach for precipitation nowcasting,” *NeurIPS*, 2015.
- [3] X. Shi, Z. Gao, L. Lausen, et al., “Deep learning for precipitation nowcasting: A benchmark and A new model,” in *NeurIPS*, 2017.
- [4] Y. Wang, M. Long, J. Wang, et al., “Predrnn: Recurrent neural networks for predictive learning using spatiotemporal lstms,” in *NeurIPS*, 2017.
- [5] Y. Wang, H. Wu, J. Zhang, et al., “Predrnn: A recurrent neural network for spatiotemporal predictive learning,” *arXiv:2103.09504*, 2021.
- [6] Y. Wang, Z. Gao, M. Long, et al., “Predrnn++: Towards A resolution of the deep-in-time dilemma in spatiotemporal predictive learning,” 2018.
- [7] Y. Wang, J. Zhang, H. Zhu, et al., “Memory in memory: A predictive neural network for learning higher-order non-stationarity from spatiotemporal dynamics,” in *CVPR*, 2019.
- [8] Y. Wang, L. Jiang, M. Yang, et al., “Eidetic 3d LSTM: A model for video prediction and beyond,” in *ICLR*, 2019.
- [9] Z. Lin, M. Li, Z. Zheng, et al., “Self-attention convlstm for spatiotemporal prediction,” in *AAAI*, 2020.
- [10] S. Bengio, O. Vinyals, N. Jaitly, et al., “Scheduled sampling for sequence prediction with recurrent neural networks,” 2015.
- [11] J. Ba, J. Kiros, and G. Hinton, “Layer normalization,” *arXiv:1607.06450*, 2016.
- [12] I. Loshchilov and F. Hutter, “Fixing weight decay regularization in adam,” *arXiv:1711.05101*, 2017.
- [13] N. Srivastava, E. Mansimov, and R. Salakhutdinov, “Unsupervised learning of video representations using lstms,” in *ICML*, 2015.
- [14] Y. Yamamoto, K. Ichii, A. Higuchi, et al., “Geolocation accuracy assessment of himawari-8/ahi imagery for application to terrestrial monitoring,” *Remote. Sens.*, 2020.
- [15] J. Hsieh, B. Liu, D. Huang, et al., “Learning to decompose and disentangle representations for video prediction,” in *NeurIPS*, 2018.
- [16] W. Yu, Y. Lu, S. Easterbrook, et al., “Efficient and information-preserving future frame prediction and beyond,” in *ICLR*, 2020.
- [17] V. Guen and N. Thome, “Disentangling physical dynamics from unknown factors for unsupervised video prediction,” in *CVPR*, 2020.
- [18] J. Donà, J. Franceschi, S. Lamprier, et al., “Pde-driven spatiotemporal disentanglement,” in *ICLR*, 2021.